

Simulation Modeling and Charge–Discharge Characteristics of a Zinc–Nickel Single-Flow Battery Stack

Xiaofei Sun¹, Shouguang Yao^{1*}, Qian Zhao¹, Yunhui Zhao¹, Jie Cheng²

¹ School of Energy and Power Engineering, Jiangsu University of Science and Technology, Zhenjiang 212003, China

² Zhangjiagang Smartgrid Fanghua Electrical Energy Storage Research Institute Co., Ltd., Zhangjiagang 215600, China

*E-mail: zjyaosg@126.com

Received: 3 September 2019 / Accepted: 29 October 2019 / Published: 30 November 2019

An equivalent circuit simulation model of a zinc–nickel single-flow battery stack that considers internal resistance loss and external parasitic loss is built by MATLAB/Simulink to accurately predict the actual operation characteristics of a zinc–nickel single-flow battery stack. The dynamic internal resistance obtained by experimental fitting is used to optimize the original simulation model and subsequently improve the accuracy of the model. Then, the performance of the battery stack with different currents is predicted and analyzed. Simulation results show that the peak of the battery terminal voltage decreases, the coulomb efficiency of the battery increases, and the voltage efficiency and energy efficiency decrease with the increase in current.

Keywords: zinc–nickel single-flow battery; equivalent circuit; electrochemical reaction; Nernst equation; simulation

1. INTRODUCTION

The realization of sustainable development of energy and the environment has been accompanied by renewable energy, as represented by solar energy and wind energy, which is highly valued by all countries in the world. In terms of solving the problems of instability of renewable energy power generation and large-scale energy storage, liquid-flow battery has attracted extensive attention due to its advantages of independent output power and capacity, long service life, deep discharge, high energy efficiency, absence of pollution, simple maintenance, low cost, safety and environmental protection, etc. [1–3]. Although many liquid-flow battery systems have been developed, only sodium polysulfide/bromine batteries, all-vanadium redox flow batteries (VRBs) [4–5], and other dual-flow batteries can enter into commercial demonstration and the operational stage at present. These batteries have entailed the problems of ion cross contamination and high price of ion exchange membranes.

Single-flow batteries have attracted considerable attention due to their advantages of single-liquid, non-membrane, or low-cost microporous membrane. Among them, the zinc–nickel single-flow battery proposed by Jie Cheng [6] has been highly commended for its long life, excellent battery efficiency, low self-discharge, good cycle performance, safety and environmental protection, and other good characteristics [7]. The external characteristics of battery stacks must be mastered to achieve the safe operation and management of large-scale energy storage systems. Therefore, the modeling and simulation of battery stacks and the accurate and effective prediction of their external characteristics have become the focus of all-liquid-flow batteries for application.

The current research on the prediction of the external characteristics of liquid-flow batteries mainly focuses on all-VRBs due to the restrictions of battery application requirements. The literature [8] established a simulation model of all-VRBs by Simulink, and a simulation study on its state of charge (SOC) and charge–discharge characteristics in the constant current charging and discharging mode was conducted to verify the accuracy of the model. The literature [9] proposed a new VRB model based on the stack efficiency curve to solve the problem in which the parameters required by the traditional model are difficult to obtain through experiments. The model was especially suitable for the dynamic study of a power system and attained better accuracy compared with experimental results. The literature [10] built an equivalent circuit model of all-VRBs based on electrolyte flow, pump loss, self-discharge, and other factors to accurately estimate the terminal voltage and the dynamic SOC of a battery stack. By investigating the optimal range of electrolyte flow under dynamic SOC, the study provided theoretical support for the design of flow controller. The literature [11] investigated the operation optimization control of all-VRBs based on an equivalent circuit model. By analyzing the influence law of the operation parameters on the performance of the battery, the study was able to prove the effectiveness of the optimized operational control.

The research on zinc–nickel single-flow battery in recent years has been mainly based on experiments [12–17], but the research on simulation modeling of the zinc–nickel single-flow battery has also achieved some progress. The literature [18] established an electrochemistry model and a mechanical model of the zinc–nickel single-flow battery based on the battery's working principle, and a simulation was carried out in the constant current charge–discharge mode. However, considering that the model did not consider ohmic resistance and polarization resistance in the process of simulation, it cannot contrast battery open circuit voltage and the terminal voltage, and it cannot clearly present the reason of the change in the battery terminal voltage curve. The literature [19] established a partnership for a new generation of vehicle (PNGV) model based on the working principle of the zinc–nickel single-flow battery. The parameters of the PNGV model were identified by parameter identification according to the experimental data of pulse discharge below 100 A, and the analytical expressions of the parameters of each model were obtained using the high-order polynomial and exponential function fitting method. The battery's characteristic parametric formula obtained by the fitting method effectively solved the problem involved in calculating the battery's characteristic parameters. The literature [20] proposed an improved Thevenin equivalent circuit model and built a simulation model in the MATLAB/Simulink environment. The comparison with experimental values showed that the improved model was more accurate than the traditional Thevenin equivalent circuit model, and it was even more precise in predicting the terminal voltage of the battery's constant current discharge.

On the basis of the preliminary work of the team, this study further considers the influence of internal resistance loss and external parasitic loss of the zinc–nickel single-flow battery stack on battery performance and further establishes an accurate prediction model for the external characterization of the zinc–nickel single-flow battery. Subsequently, the effects of different constant currents on the charge–discharge process is analyzed to provide reference for further research and the operational control optimization of the zinc–nickel single-flow battery.

2. WORKING PRINCIPLE AND EQUIVALENT CIRCUIT MODEL OF ZINC–NICKEL SINGLE-FLOW BATTERY

2.1 Working principle of zinc–nickel single-flow battery

Fig. 1 shows the schematic diagram of the working principle of a zinc–nickel single-flow battery. A pump drives the circulation of high-concentration zincate alkaline electrolyte between the battery and the liquid storage tank. During the charging process, the deposited zinc is attached to the negative electrode plate, and the nickel hydroxide in the porous positive electrode plate is oxidized to the nickel oxide hydroxide and water. During the discharging process, the zinc of the negative electrode plate is oxidized, and the active substance of the positive electrode changes from nickel oxide hydroxide to nickel hydroxide.

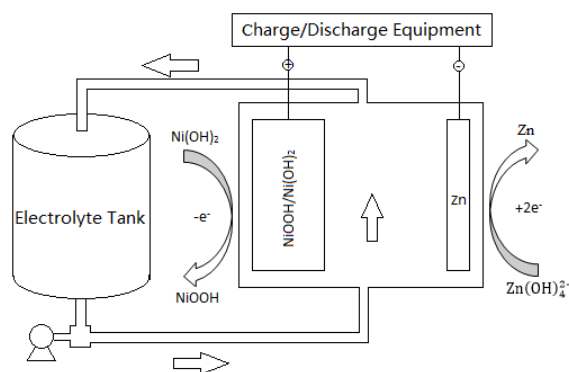


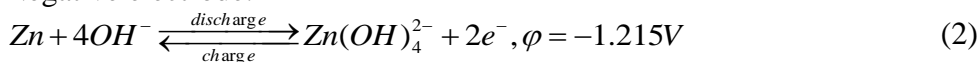
Figure 1. Schematic diagram of a zinc–nickel single-flow battery

The electrode chemical reactions are as follows:

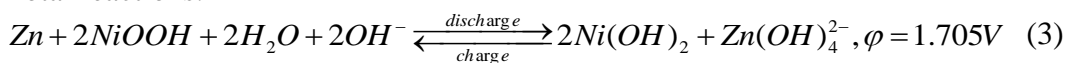
Positive electrode:



Negative electrode:



Total reactions:



2.2 Equivalent circuit model of the zinc–nickel single-flow battery

A good equivalent circuit model must meet the following criteria: (1) the model can accurately present the inputted and outputted volt–ampere characteristics and the energy loss of the battery, and (2) the complexity of the model is not exceptionally high. The literature [18] used Simulink to simulate the charge–discharge process of a zinc–nickel single-flow battery. However, the external parasitic loss (fixed resistance loss or pump loss) during battery operation was not analyzed in detail, and the model did not include the overall system. On the basis of the method of work in the literature [18], this study further considers the effects of equivalent parallel resistance and equivalent parasitic loss and pump loss on battery terminal voltage and battery system power. The equivalent circuit model of the zinc–nickel single-flow battery is shown in Fig. 2. In the figure, R_{rea} is the sum of the activation polarization resistance and the concentration polarization resistance, R_{res} is the ohmic resistance, and R_{fix} is the internal fixed loss of the battery. The model is used to compare the stack voltage with the terminal voltage of the batteries, and the calculation of the battery system power and the pump loss current is also improved accordingly.

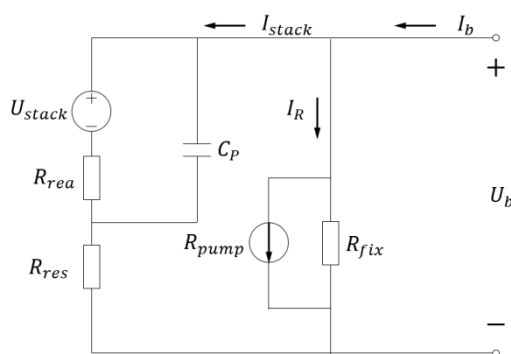


Figure 2. Equivalent circuit model

3. SIMULATION MODEL OF THE ZINC–NICKEL SINGLE-FLOW BATTERY STACK

3.1 Electrochemical model of the zinc–nickel single-flow battery

3.1.1 Polarization distribution in the battery

Three main processes (ohmic polarization, activation polarization, and concentration polarization) lead to overpotential during battery operation. These processes can be described as follows. (1) Electrode resistance and electrolyte resistance hinder the flow of charge. The obstructed flow affects battery voltage and produces ohmic polarization overpotential. (2) In electrochemical reactions, a slow reaction rate on the surface of the electrode leads to the generation of activated polarization overpotential. (3) When current passes through a battery, a concentration gradient is generated between the electrolyte solution and the electrode surface. Meanwhile, in the process of reaction, the diffusion rate of the reactant diffusing from the bulk solution to the electrode surface is lower than the consumption rate of the reactant on the electrode surface, thereby generating a concentration polarization

overpotential. These three types of overpotential cause energy losses, resulting in certain differences between the battery stack voltage U_{stack} and the terminal voltage U_b .

3.1.2 Stack analysis of the battery

According to Nernst equation in chemistry, the battery stack potential can be obtained as follows:

$$U_{stack} = U_0 + \frac{RT}{2F} \ln \left\{ \frac{[NiOOH]^2 \cdot [OH^-]^2}{[Ni(OH)_2]^2 \cdot [Zn(OH)_4^{2-}]} \right\}, \quad (4)$$

where U_0 is the standard voltage (1.705 V), R is the gas constant (8.314 J/K·mol), T is the temperature (298 K), F is the Faraday constant (96485 C·mol⁻¹), and $[i]$ is the concentration of substance i .

The SOC of a battery is the state parameter that represents the residual energy in the battery, and it indicates the ratio of the residual capacity to the rated capacity.

$$SOC = \frac{\text{residual capacity}}{\text{rated capacity}}, \quad (5)$$

$$SOC = SOC_0 + \int \frac{I_{stack} U_{stack}}{P_{rate} T_{rate}} dt, \quad (6)$$

where T_{rate} is the time when the energy storage system charges from the SOC of 0% to 100% at the rated power P_{rate} . I_{stack} is positive when charging and negative when discharging.

Given that SOC is affected by ion concentration, the relationship between stack voltage U_{stack} and SOC can be obtained by derivation.

$$U_{stack} = U_0 + \frac{RT}{2F} \ln \left(\left(\frac{SOC}{1-SOC} \right)^2 \cdot \frac{(1.4SOC+9.6)^2}{1-0.7SOC} \right) \quad (7)$$

Battery terminal voltage is mainly determined by the electromotive force and the internal voltage loss of the zinc–nickel single-flow battery stack.

$$U_b = U_{stack} \pm U_{loss} \quad (8)$$

3.2 Mathematical model of the zinc–nickel single-flow battery

3.2.1 Calculation of internal loss and external parasitic loss of the battery

Internal loss and external parasitic loss occur during battery operation. The experiments indicate that the energy loss η_{loss} of the battery stack (300 Ah) is 31% when the charge–discharge current is 100 A.

The actual power inside the battery is given by the following formula:

$$P_{stack} = \frac{P_{rate}}{1-\eta_{loss}}. \quad (9)$$

The ohmic loss coefficient and the polarization loss coefficient k are given by the following formula:

$$R = \frac{k \cdot P_{stack}}{I_{max}^2}. \quad (10)$$

In the literature [19], the experimental calculations of ohmic resistance R_{res} and polarization resistance R_{rea} are 0.623 mΩ and 0.2504 mΩ, respectively. According to Eq. (10), the equivalent internal resistance loss coefficient during battery operation is 13.8%, of which 10.35% is caused by R_{res} , and 3.45% is caused by R_{rea} . The external parasitic loss is 17.2%, including fixed resistance loss R_{fix} and pump loss R_{pump} .

External parasitic loss can be expressed as

$$P_{parasitic} = P_{fix} + P_{pump} = P_{fix} + K \left(\frac{I_{stack}}{SOC} \right), \quad (11)$$

$$I_{pump} = \frac{P_{pump}}{V_b} = \frac{K \left(\frac{I_{stack}}{SOC} \right)}{V_b}, \quad (12)$$

where V_b is the terminal voltage during battery operation, and K is related to the pump loss constant.

3.2.2 Calculation of mechanical loss of the battery

A certain mechanical loss occurs in the process of battery operation. The mechanical loss mainly consists of two parts: (1) the power P_{pipe} consumed by the electrolyte flowing through the pipe connected to the stack and external storage tank and (2) the mechanical loss P_{stack} caused by pressure drop when the electrolyte flows through the stack.

The mechanical loss of the whole battery system is given as follows:

$$P_{mech} = \frac{\Delta P \cdot Q}{\eta}. \quad (13)$$

For a given pump, the pump efficiency η is constant, where $\eta = 80\%$. ΔP is the loss of the electrolyte in the flow ($\Delta P = \Delta P_{pipe} + \Delta P_{stack}$), and Q is the loss of electrolyte in the flow and the flow rate of the electrolyte, respectively.

The loss of electrolyte in the flow passage can be expressed as follows:

$$-\Delta P_{pipe} = \rho g h_f + \rho g h_m + \rho g \Delta z + \rho g \frac{\Delta v^2}{2g}, \quad (14)$$

that is,

$$\Delta P_{pipe} = -\rho g \left(h_f + h_m + \Delta z + \frac{\Delta v^2}{2g} \right), \quad (15)$$

where ρ is electrolyte density; h_f is the loss along the pipeline ($h_f = \lambda \frac{L}{D} \cdot \frac{v^2}{2g}$); h_m is the local loss in the pipeline ($h_m = k \frac{v^2}{2g}$); Δz is the height difference between the inlet and the outlet of the pipeline; and Δv is the difference in velocity between the two ends of the pipeline.

The pressure drop in the solution of the stack is determined by electrolyte flow and electrolyte resistance. The pressure drop in the stack is expressed as follows:

$$\Delta P_{stack} = Q \cdot \tilde{R}, \quad (16)$$

where \tilde{R} is the fluid resistance of the stack. Here, we take the value of $\tilde{R} = 14186843 \text{ Pa/m}^3$ in the literature [17].

3.3 Simulation model and verification of the battery

This study regarded the zinc–nickel single-flow battery stack with a rated power of 160 W and a rated charge–discharge capacity of 300 Ah as the research object. The charge–discharge characteristics of the battery system were simulated using Simulink. The main parameters used in the simulation process are shown in Table 1.

Table 1. Original Data of Simulation.

Name	Value
T	298 K
C_{max}^H	35.3 mol/L
$C_{Zn(OH)_4^{2-}}$ (when charge begins)	1 mol/L
$C_{Zn(OH)_4^{2-}}$ (when charge ends)	0.3 mol/L
C_{OH^-} (when discharge begins)	11 mol/L
C_{OH^-} (when discharge ends)	9.6 mol/L
R_{res}	0.00062 Ω
R_{rea}	0.00025 Ω
R_{fix}	0.313 Ω
C_p	138 F
η	0.8
ρ	1456.1 kg/m ³

A charge–discharge simulation model of the zinc–nickel single-flow battery system is established in Simulink, as shown in Fig. 3. The zinc–nickel single-flow battery is charged and discharged at a constant current of 100 A. The effectiveness of the model is verified by comparing the simulation results with the experimental results, as shown in Fig. 6(a). The simulated data agree well with the experimental data, but the initial and final errors between charging and discharging are large. The main reason is that self-discharge was not considered, thus resulting in certain errors. The application of the Nernst equation was also limited in the initial and final stages of the charge and discharge process. In addition, the ohmic resistance and the polarization resistance are set with fixed values. The increase in ohmic resistance and the polarization phenomenon were both ignored in the process of battery operation, thus resulting in relatively large errors in the discharge process.

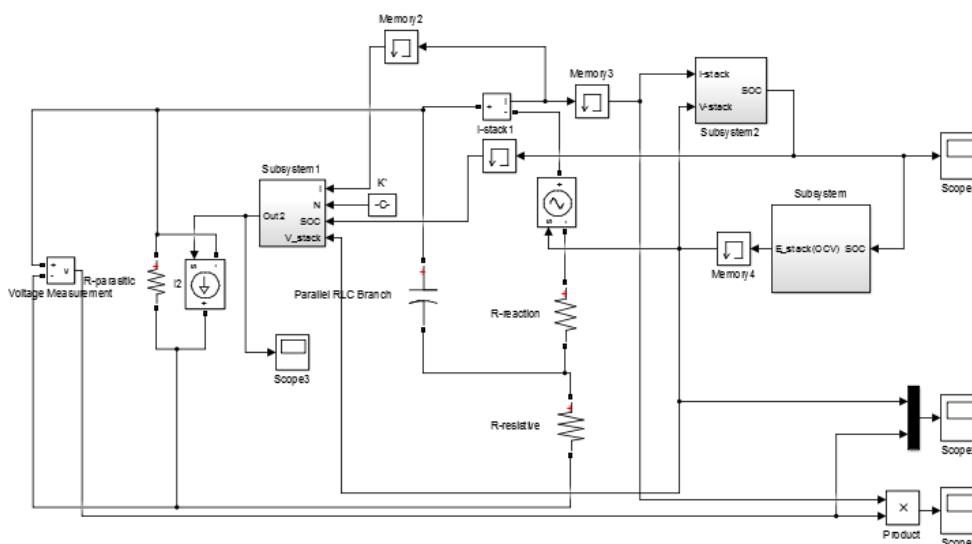


Figure 3. Simulation model of the battery

According to the literature [19], the fitting formula of resistance in the discharge process as a means to solve the above problem is as follows:

(1) The function of ohmic internal resistance R_{res} that varies with time is

$$R_{res}(t) = 6.058 \times 10^{-4} \exp(1.853 \times 10^{-5}t) + 2.228 \times 10^{-19} \exp(3.767 \times 10^{-3}t). \quad (17)$$

(2) The function of polarization internal resistance R_{rea} that varies with time is

$$R_{rea}(t) = 2.229 \times 10^{-4} \exp(6.543 \times 10^{-5}t) + 4.398 \times 10^{-19} \exp(3.8 \times 10^{-3}t). \quad (18)$$

The fixed resistance in the above model is changed to dynamic resistance by using a controlled current source, as shown in Fig. 4. An improved discharge simulation model is further built for the discharge process, as shown in Fig. 5. In this manner, the polarization variation trend in the actual operation process can be determined.

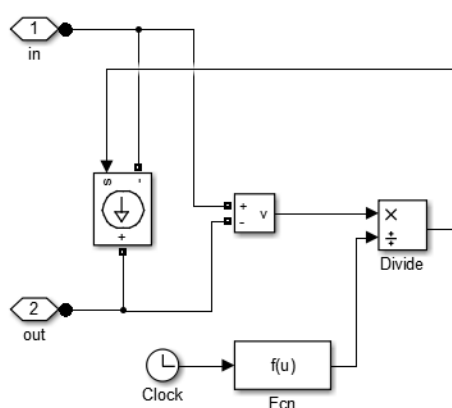


Figure 4. Simulation model of dynamic resistance of the battery

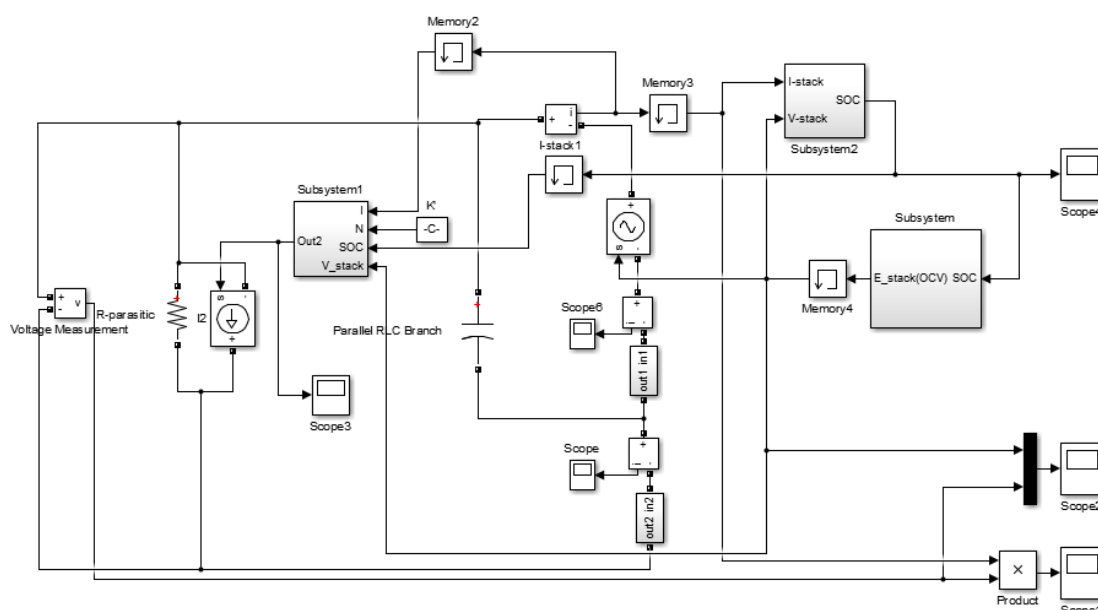


Figure 5. Improved discharge simulation model of the battery

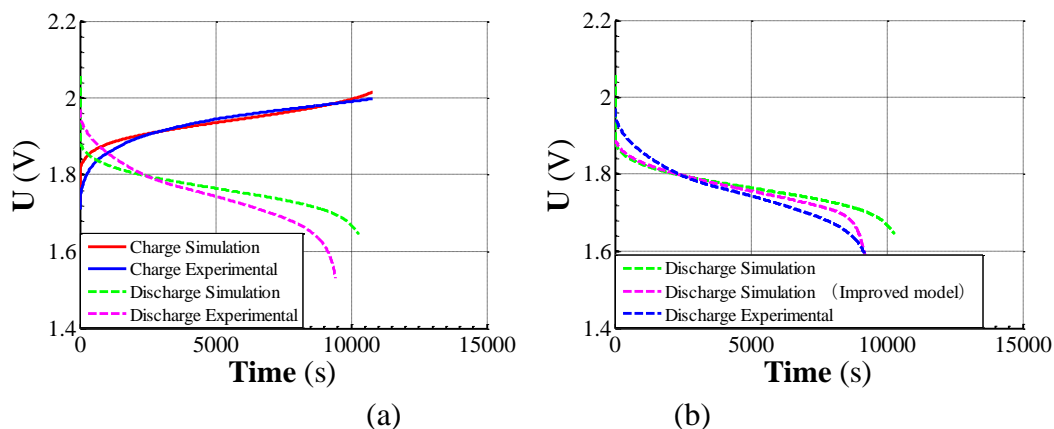


Figure 6. Simulation and experimental curves of the stack voltage

The comparative results between the simulation and the experimental of the original model, as shown in Fig. 6(b), indicate a smaller relative error for the simulation results of the improved model. This finding implies that the dynamic variation in ohmic resistance and polarization resistance has a certain influence on terminal voltage in the actual discharge process.

The model in the literature [18] represent a battery stack with a rated charge–discharge capacity of 216 Ah. Meanwhile, the model in this study has a rated charge–discharge capacity of 300 Ah, as shown in Fig. 7. In the literature [18], the relative error of terminal voltage is 4% between the simulation value and the experimental value in general; however, the relative error of the terminal voltage was 8.7% at the end of battery discharge. By using the simulation model established in this study, the relative error of terminal voltage was notably reduced. As shown in Fig. 8, the relative error of the whole operation process is nearly 3%. In contrast with the literature [18], the influences of equivalent parallel resistance and equivalent parasitic loss and pump loss on battery terminal voltage are considered in the model established in this study. Consequently, the model in this study is highly accurate and suitable for performance prediction and analysis of the zinc–nickel single-flow battery stack.

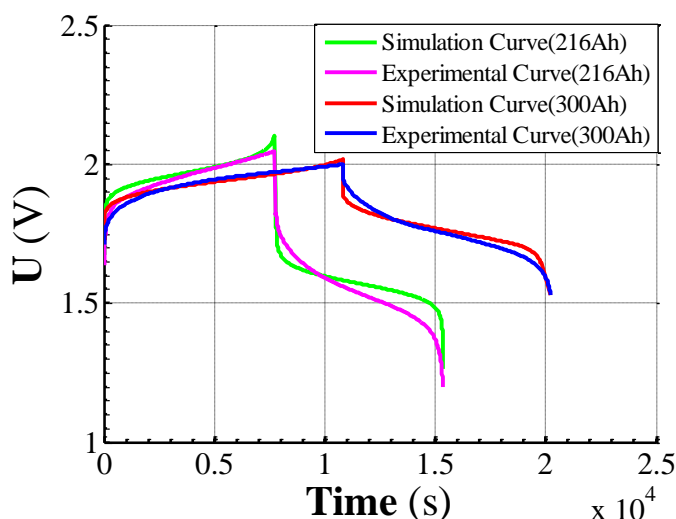


Figure 7. Simulation curve and experimental curve of battery stack voltage with different rated charge–discharge capacities

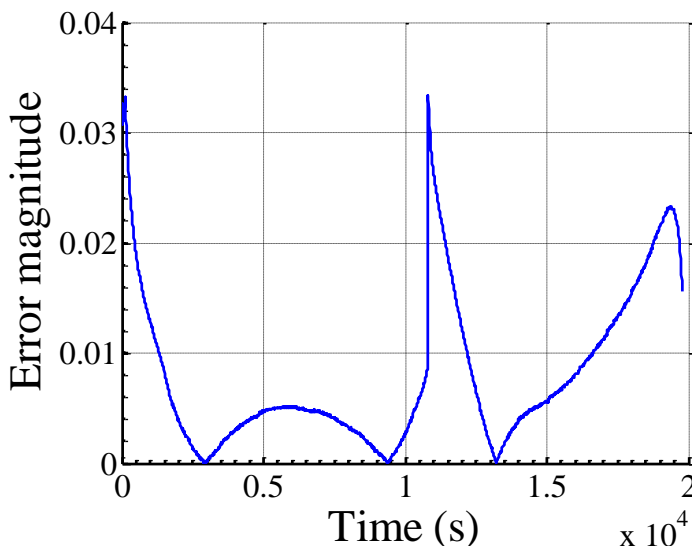


Figure 8. Relative error curves over time

4. ANALYSIS OF CHARGE–DISCHARGE CHARACTERISTICS OF THE ZINC–NICKEL SINGLE-FLOW BATTERY STACK

4.1 Charge–discharge characteristics of the battery stack

The charge–discharge characteristics of the zinc–nickel single-flow battery stack are determined according to the simulation model of the charge–discharge process of the established battery (Figs. 3 and 5). The power, terminal voltage, and stack voltage of the battery stack during operation at a constant current of 100 A are also investigated.

Fig. 9 shows that the change in SOC over time for the charge–discharge process of the zinc–nickel single-flow battery stack. The duration is approximately 6 h.

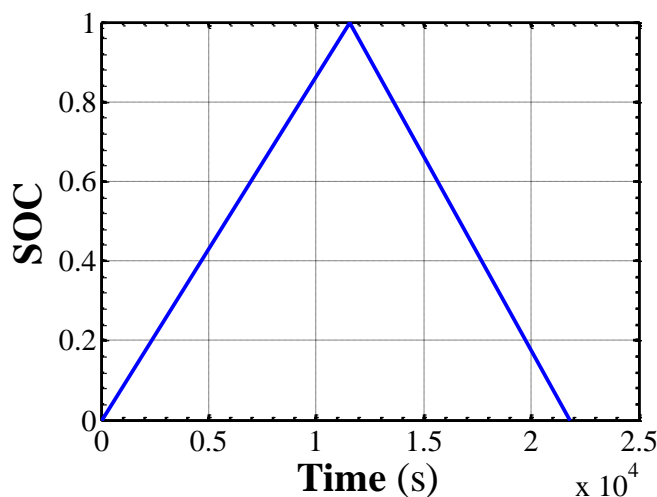


Figure 9. Simulation curves of SOC

Fig. 10 shows the curve of the absorption or release power of the battery stack over time during the charge–discharge process. The power of the battery stack is always smaller than the actual power P_{stack} (232 W) during charging. This phenomenon is due to the energy consumption of the ohmic resistance, polarization resistance, and external parasitic loss of the battery, thus resulting in energy loss of the stack in the process of operation. In the literature [20], our team constructed a general electric model of 300 Ah zinc–nickel single–flow battery. The simulation results show that when the stack is charged and discharged at 100A current, the absorption power and release power of the stack are between 175W and 200W, which is in good agreement with the simulation results in this paper.

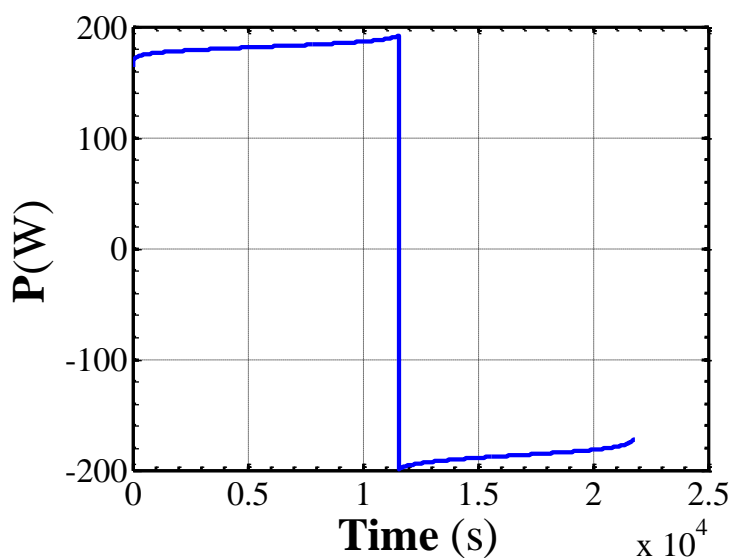


Figure 10. Simulation curves of power

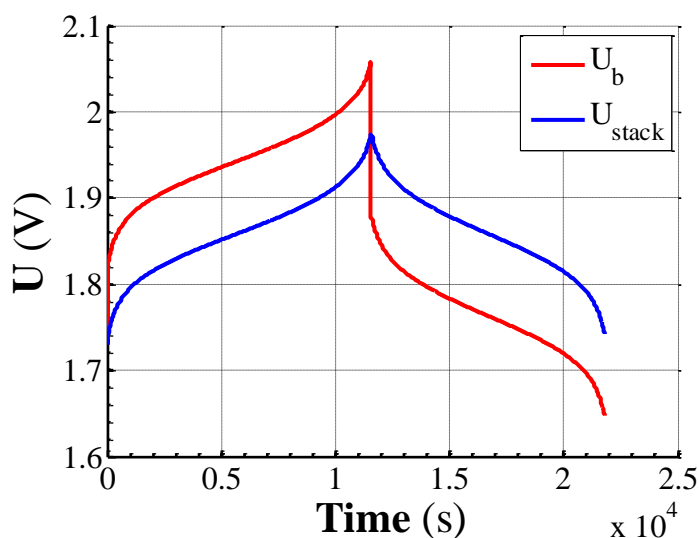


Figure 11. Comparison of curves between terminal voltage and stack voltage

Fig. 11 shows the graph of terminal voltage and stack voltage that vary with time in a charge–discharge cycle. From the simulation results, a certain difference exists between battery terminal voltage and stack voltage. Owing to the change in current direction during the charge–discharge conversion, the voltage loss U_{loss} for the equivalent internal resistance changes correspondingly, resulting in a sudden voltage drop, which renders the terminal voltage U_b of the system larger than the stack voltage U_{stack} during the charge process. Upon discharge, U_b becomes smaller than U_{stack} .

4.2 Influence of charge–discharge current on battery voltage

Figs. 12 and 13 show the changes in terminal voltage and stack voltage of the zinc–nickel single-flow battery over time. When the rated charge–discharge capacity remains unchanged, the battery is charged and then discharged at the three different constant current currents of 50, 100, and 150 A. With the increase of constant charge–discharge current, the time for the battery stack to perform a charge–discharge cycle is substantially decreased. The change in charge–discharge current does not affect the peak value of the battery stack voltage and instead causes the peak value of the battery terminal voltage to decrease continuously. The reason is that the battery stack voltage is unaffected by the charge–discharge current and instead is related to the battery material and the charged-state SOC. When the charged-state SOC remains the same, the U_{stack} also remains unchanged. However, the voltage loss U_{loss} inside the battery increases with the rise in current, which then causes the peak value of the terminal voltage U_b to decrease continuously.

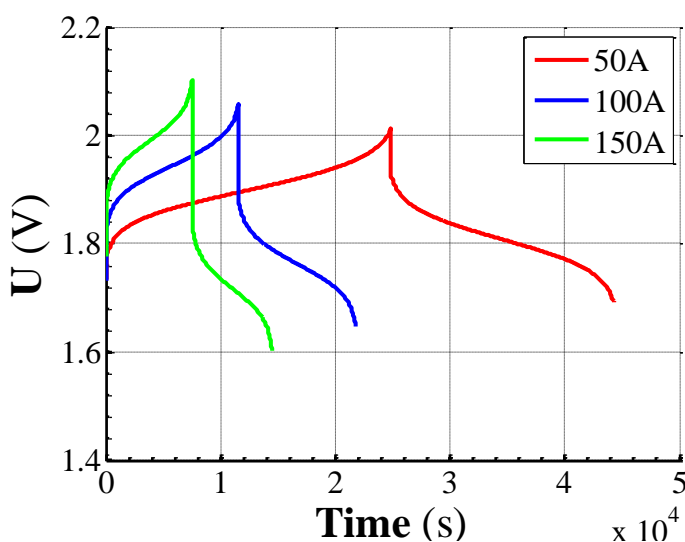


Figure 12. Terminal voltage over time with diverse currents

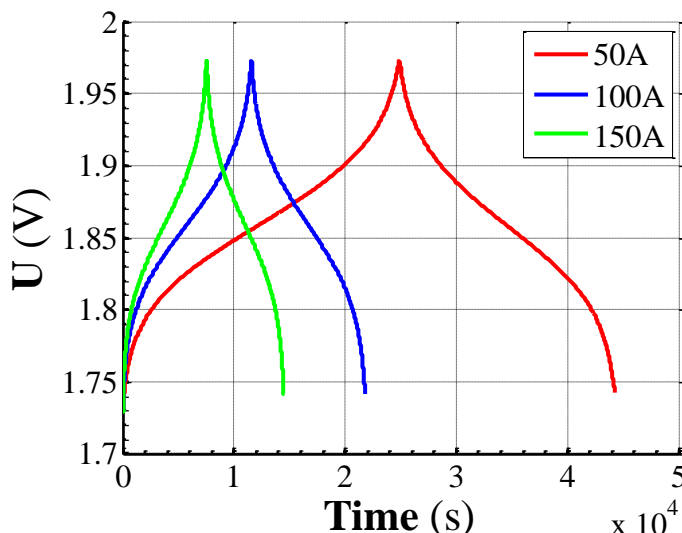


Figure 13. Stack voltage over time with diverse currents

Table 2 compares the simulated values of the average voltage and average power under different current density operating conditions with the experimental values in literature [21]. Under different current densities, the average voltage error during charging and discharging is within 0.011V, and the average power error is within 2W.

Table 2. Comparison of experimental and simulated values of average voltage and average power.

Current(A)	Average charging voltage(V)	Average discharging voltage(V)	Average absorption power(W)	Average release power(W)
Simulation results				
50	1.8901	1.6159	86	81
100	1.9565	1.5638	162	156
150	2.0299	1.5136	238	235
Experimental results in literature [21]				
50	1.8919	1.6200	88	81
100	1.9643	1.5528	163	155
150	2.0366	1.5057	239	233

4.3 Influence of charge–discharge current on energy storage efficiency

Energy storage efficiency is an important indicator of battery performance. This parameter includes coulomb efficiency E_C , energy efficiency E_E , and voltage efficiency E_V . The corresponding expressions are as follows:

$$E_C = \frac{\int I_{discharge} dt}{\int I_{charge} dt}, \tag{19}$$

$$E_E = \frac{\int U_{discharge} I_{discharge} dt}{\int U_{charge} I_{charge} dt}, \tag{20}$$

$$E_V = \frac{\bar{U}_{discharge}}{\bar{U}_{charge}}. \tag{21}$$

The performances of the zinc–nickel single-flow battery vary in different charging and discharging modes. Fig. 14 shows the coulomb efficiency, energy efficiency, and voltage efficiency of the battery charged and discharged with four different constant current currents. Coulomb efficiency increases with the rise in charge–discharge current because this increase in current shortens the time to complete a charge–discharge cycle. With the increase in charge–discharge current, the diffusion rate of the reactant diffusing from the bulk solution to the electrode surface becomes lower than the consumption rate of the reactant. The slow diffusion causes the concentration gradient to increase, thus increasing the concentration polarization overpotential. Consequently, energy efficiency and voltage efficiency decrease with the increase in charge–discharge current. The dotted line in Fig. 14 is the energy storage efficiency of batteries measured by Yao Shouguang [22] based on 300 Ah zinc–nickel single-flow battery stack with different currents. It can be found that the energy storage efficiency obtained in this paper is in good agreement with the literature values.

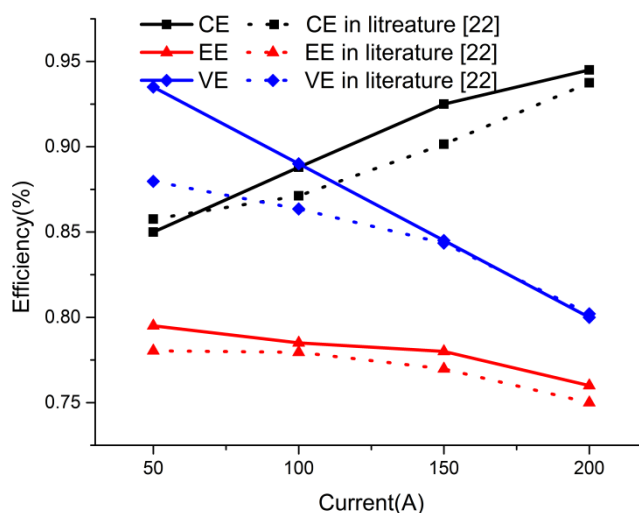


Figure 14. Energy storage efficiency at diverse currents

5. CONCLUSION

Internal resistance loss and external parasitic loss are considered in the charge–discharge simulation model of the battery stack based on the electrochemical reaction principle and the Nernst equation of the zinc–nickel single-flow battery. Then, the improved discharge simulation model is established. The characteristics of the battery stack in different charge–discharge conditions are simulated by Simulink. The following conclusions are drawn:

(1) Given that terminal voltage in the process of battery operation is affected by ohmic resistance and the polarization phenomenon, the discharge simulation model of the battery stack can be improved using the dynamic internal resistance coupling of the discharge process, which is obtained by experimental fitting. This approach can accurately reflect the discharge process of the zinc–nickel single-flow battery stack.

(2) Moreover, considering that stack voltage U_{stack} is affected by SOC in the process of constant current charge–discharge, the time needed to complete the charge–discharge cycle can be shortened with the increase in current. However, the peak value remains unchanged given the same SOC condition. Meanwhile, internal loss increases with the increase in current, which then leads to the decrease in the peak value of the battery terminal voltage U_b .

(3) With the increase in current in the constant current charge–discharge process, the time needed to complete the charge–discharge cycle is shortened, which then leads to the increase in Coulomb efficiency and the deterioration of polarization. The phenomenon of deteriorated polarization leads to the increase in internal loss, which results in a downward trend in energy efficiency and voltage efficiency.

ACKNOWLEDGEMENT

This article is funded by the National Natural Science Foundation of China (No. 51776092)

References

1. Y.H. Wen, J. Cheng, Y. Xu, G.P. Cao and Y.S. Yang, *Chemistry*, 74 (2011) 587.
2. H.M. Zhang, *Functional Materials*, 9 (2012) 7.
3. J.R. Miller, *Science*, 335 (2012) 1312.
4. P. Zhao, H.T. Zhou, H.M. Zhang and B.L. Yi, *Battery*, 34 (2004) 321.
5. L.L. Yang, W.J. Liao, Q. Su and Z.J. Wang, *Energy Storage Science and Technology*, 2 (2013) 140.
6. J. Cheng, L. Zhang, Y.S. Yang, Y.H. Wen, G.P. Cao and X.D. Wang, *Electrochemistry Communications*, 9 (2007) 2639.
7. P.C. Zhao, J. Cheng, Y. Xu, Y.H. Wen, K. He and G.P. Cao, *Summary of the 29th Annual Academic Conference of the Chinese Chemical Society*, 2014.
8. X.M. Wang, Q.L. Li and Y.M. Guo, *Power Technology*, 2 (2013).
9. L.J. Ontiveros and P.E. Mercado, *Int. J. Hydrogen. Energy*, 39 (2014) 8720.
10. A. Bhattacharjee and H. Saha, *J. Energy. Storage*, 13 (2017) 220.
11. X.N. Chi, M.G. Zhu and Q.X. Wu, *Energy Storage Science and Technology*, 7 (2018) 503.
12. J. Cheng, Y.H. Wen, G.P. Cao and Y.S. Yang, *J. Power Sources*, 196 (2011) 1589.
13. I. Yasumasa, N. Michael, P. Robert, K. Martin and B. Sanjoy, *J. Power Sources*, 196 (2011) 6583-6587.
14. Y.H. Wen, T. Wang, J. Cheng, J.Q. Pan, G.P. Cao and Y.S. Yang, *Electrochim. Acta*, 59 (2012) 64.
15. Y.H. Cheng, H.M. Zhang, Q.Z. Lai, X.F. Li and D.Q. Shi, *Electrochim. Acta*, 105 (2013) 618.
16. Y.H. Cheng, H.M. Zhang, Q.Z. Lai, X.F. Li and D.Q. Shi, *J. Power Sources*, 241 (2013) 196.
17. Y.H. Cheng, H.M. Zhang, Q.Z. Lai, X.F. Li, Q. Zheng, X.L. Xi and C. Ding, *J. Power. Sources*, 249 (2014) 435.
18. S.G. Yao, P. Liao, M. Xiao, J. Cheng, and K. He, *AIP. Adv.*, 6 (2016) 125302.
19. S.G. Yao, P. Liao, M. Xiao, J. Cheng, and K. He, *AIP. Adv.*, 7 (2017) 1.
20. S.G. Yao, X.F. Sun, M. Xiao, J. Cheng and Y.J. Shen, *Energies*, 12 (2019) 582.
21. Y.X. Li, M.C. Wong, W.F. Ip, P.C. Zhao and Z.Y. You, *IEEE 9th Conference on Industrial Electronics and Applications (ICIEA)*, 2014.
22. S.G. Yao, P. Liao, M. Xiao, J. Cheng, and W.W. Cai, *Int. J. Electrochem. Sci.*, 13 (2018) 4455.